

Combustion and Emission Performance in a Can Annular Combustor

Gang Pan, Hongtao Zheng

Abstract—In order to design a dual-fuel combustor for the Chemically Recuperated Gas Turbine (CRGT), numerical research on the performance of a can annular combustor is presented in this paper. The objective is to understand the impact of different actual operating conditions on combustion and emission performance. The load of the combustor is varied from 30% to 100%. The mathematical models used for fuel combustion consist of the realizable k - ϵ model for turbulent flow, discrete phase model (DPM) for tracking the oil droplet path lines, probability density function (PDF) model for non-premixed oil combustion and pollution model for nitrogen oxides (NO_x) emission. The obtained results using these models show good agreement with other experimental results. The effects of different conditions on the flow field, flame shape, gas temperature and NO_x emission are presented in this paper. The results obtained in this study show the change in gas turbine can annular combustor performance with different actual operating conditions.

Index Terms—Numerical simulation, different conditions, flow field, NO_x emission

I. INTRODUCTION

GAS turbines that operate in simple cycles have low efficiencies because the turbine exhaust gases come out very hot and this energy is lost to the atmosphere [1]. In order to recuperate of the exhaust energy from gas turbines, the CRGT system has been presented. Concerning CRGT systems, there are some reports on the thermal efficiency and feasibility of the systems [1]-[4]. But few literatures exist on the combustor design which is a major problem in developing a CRGT system. The combustor is the most heavily thermal load part in the gas turbine, in which both ignition and combustion keep going on, and normally whose service life is very short [5]. The performance of the CRGT, particularly the operating efficiency and reliability would be great affected by the combustor. In order to shorten the design period and increase the design efficiency, a method of modifying an original oil fuel combustor into a dual-fuel one is adopted in this paper. In order to design a dual-fuel combustor with good performance, it is necessary to study the performance of the original oil fuel combustor under different operating conditions.

With the development of computer technology, the method

of numerical simulation is more and more employed to study the turbulent flow in different fields [5]-[7]. So far there are very plenty of available researchers have employed CFD to investigate the flow, combustion and heat transfer in a combustor. For example, Li et al. [5] made use of the CFD method to analyze combustion and cooling performance in an aero-engine combustor. Wang et al. [8] studied the structure of a hydrogen/air premixed flame in a micro combustor under one condition by the direct numerical simulation method. Gobbato et al. [9] performed a CFD simulation on a hydrogen fuelled single can gas turbine combustor. Ghenai [10] carried out a numerical investigation on the combustion of syngas fuel mixture in gas turbine can combustor. The effects of syngas fuel composition and lower heating value on the flame shape, gas temperature, and nitrogen oxides per unit of energy generation were presented. Orbay et al. [11] employed the LES model to study the swirling isothermal and reactive flows of premixed natural gas/air mixture in a laboratory combustion chamber. Wan et al. [12] investigated the effects of the inlet velocity and equivalence ratio on the blow-off limit, combustion efficiency, exhaust gas temperature and outer wall temperature profile numerically. Zhang et al. [13] studied the NO_x emission in a model commercial aircraft engine combustor by the CFD approach. Hu et al. [14] proposed a new methodology named FIA (fuel iterative approximation) for LBO limit predictions of combustors, and then the CFD was employed to predict the LBO limits for an aero-engine combustor. However, all above-mentioned studies on the performance of combustor with different geometric structures or inlet parameters under constant load, but a limited number of people have studied the performance of a can annular combustor under different actual operating conditions.

In this paper, in order to modify the original oil fuel combustor into a dual-fuel one, the numerical simulation is adopted to study the performance of the oil combustor under different actual operating conditions in detail. And the velocity field, temperature field, pressure loss, NO_x emission and so on are obtained and analyzed.

II. GOVERNING EQUATIONS

The mathematical equations describing the oil combustion are based on the equations of conservation of mass, momentum, and energy together with other supplementary equations for the turbulence and combustion. The realizable k - ϵ turbulence model is used in this study. The equations for the turbulent kinetic energy k and the dissipation rate of the turbulent kinetic energy ϵ are solved. For non-premixed combustion modeling, the PDF model is used. The equations

Gang Pan is with the College of Power and Energy Engineering, Harbin Engineering University, Harbin 150001, Heilongjiang, China. (e-mail: markpg0808@gmail.com).

Hongtao Zheng is with the College of Power and Energy Engineering, Harbin Engineering University, Harbin 150001, Heilongjiang, China. (e-mail: zhenghongtao9000@163.com).

are as follows (ignore radiation and gravitation) [15]:

Mass Conservation Equation:

$$\nabla \cdot (\rho \bar{V}) = S_m \quad (1)$$

Where the S_m is the mass added to the continuous phase from the dispersed second phase.

Momentum Conservation Equation:

$$\nabla \cdot (\rho \bar{V} \bar{V}) = -\nabla p + \nabla \cdot \bar{\tau} + \bar{F} \quad (2)$$

Where $\bar{\tau}$ and \bar{F} are the stress tensor, force between dispersed second phase and continuous phase, respectively.

Energy Conservation Equation:

$$\nabla \cdot (\rho \bar{V} E) = \nabla \cdot \left(k_{eff} \nabla T - \sum_{i=1}^{N_s} h_i \bar{J}_i + \bar{\tau} \cdot \bar{V} - p \bar{V} \right) + S_h + q_D \quad (3)$$

Where k_{eff} , \bar{J}_i , S_h and q_D are the effective conductivity, diffusion flux of species i , heat of chemical reaction, heat exchanger between dispersed second phase and continuous phase, respectively.

Particles Motion Equation:

$$\frac{d\bar{V}_p}{dt} = F_D (\bar{V} - \bar{V}_p) + \bar{F}_x \quad (4)$$

Where \bar{F}_x is an additional acceleration (force/unit particle mass) term.

PDF Combustion Model:

$$\nabla \cdot (\rho \bar{V} \bar{f}) = \nabla \cdot \left(\frac{\mu_t}{\sigma_f} \nabla \bar{f} \right) + S_m \quad (5)$$

$$\nabla \cdot (\rho \bar{V} \bar{f}^2) = \nabla \cdot \left(\frac{\mu_t}{\sigma_f} \nabla \bar{f}^2 \right) + C_g \mu_t (\nabla \bar{f})^2 - C_d \rho \frac{\varepsilon}{k} \bar{f}^2 \quad (6)$$

Where \bar{f} and \bar{f}^2 are the mixture fraction and mixture fraction variance, respectively. The constant values of σ_f , C_g and C_d are 0.85, 2.86 and 2.0, respectively.

Realizable k- ε model:

$$\nabla \cdot (\rho \bar{V} k) = \nabla \cdot \left(\left(\mu + \frac{\mu_t}{\sigma_k} \right) \nabla k \right) + G_k + G_b - \rho \varepsilon - Y_k + S_k \quad (7)$$

$$\nabla \cdot (\rho \bar{V} \varepsilon) = \nabla \cdot \left(\left(\mu + \frac{\mu_t}{\sigma_\varepsilon} \right) \nabla \varepsilon \right) + \rho C_1 S \varepsilon - \rho C_2 \frac{\varepsilon^2}{k + \sqrt{\nu \varepsilon}} + C_{1\varepsilon} \frac{\varepsilon}{k} C_{3\varepsilon} G_b + S_\varepsilon \quad (8)$$

Where the $\sigma_k=1.0$, $\sigma_\varepsilon=1.2$, $C_{1\varepsilon}=1.44$, $C_2=1.9$.

III. GEOMETRY, BOUNDARY CONDITIONS, MESH, AND NUMERICAL METHOD

The gas turbine can annular combustor is designed to burn

the fuel efficiently. The basic geometry of the gas turbine can annular combustor is shown in Fig. 1(a). The size of the combustor is 0.391m in the Z direction, 0.245m in the Y direction, and 0.743m in the X direction. A quality mesh was generated for the can annular combustor (see Fig. 1(b)).

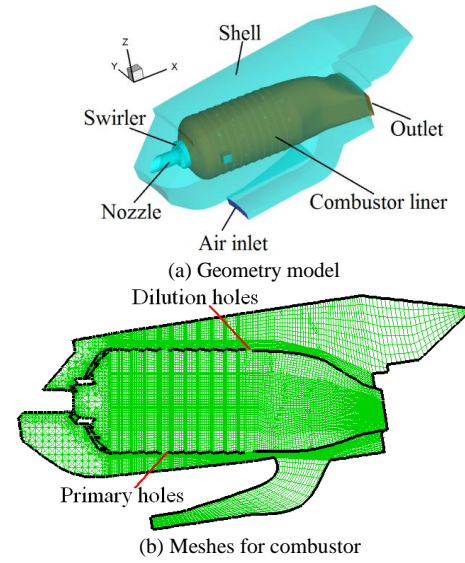


Fig. 1. Geometry and meshes of the gas turbine can annular combustor

The finite volume method and the first-order upwind method were used to solve the governing equations. The convergence criteria were set to 10^{-4} for the mass, momentum, turbulent kinetic energy, dissipation rate of the turbulent kinetic energy, and the mixture fraction. For the energy and the pollution equations, the convergence criteria were set to 10^{-6} . The boundary conditions of the air and oil are shown in Table I.

TABLE I
CONDITIONS IN COMBUSTOR

Conditions	A	B	C	D	E
Combustor load (%)	30	50	70	80	100
Air mass flow rate (kg/s)	2.7568	3.3458	3.8069	4.016	4.3865
Air Temperature (K)	645.4	693.2	726.8	742	769.9
Air pressure (MPa)	1.13196	1.4447	1.70289	1.82633	2.05344
Oil mass flow rate (kg/s)	0.04184	0.05939	0.07552	0.08382	0.09987
Oil Temperature (K)	300	300	300	300	300

IV. MODEL VALIDATION

The experimental data of [16] was used to validate the numerical model. In the experimental and numerical cases, the fuel of aviation kerosene and $C_{12}H_{23}$ were adopted, respectively. The boundary conditions of the experimental and numerical cases are as follows: air mass flow rate, 0.24kg/s, the temperature is 500K, the pressure is 0.13 MPa; oil mass flow rate, 0.00624kg/s, the temperature is 300K.

The temperature and CO_2 mass fraction radial profiles at the combustor outlet are compared to the results of [16] in

Fig.2, respectively. The values of temperature and CO₂ mass fraction in the present results and the experimental results of [16] are completely similar. The tiny differences between the experimental and numerical results may be due to the alternative fuel adopted in the numerical case and the measurement error in the experimental case. Based on the comparisons, the obtained profiles have an accepted behavior and accuracy; thus the solution can appropriately study the performance of combustor.

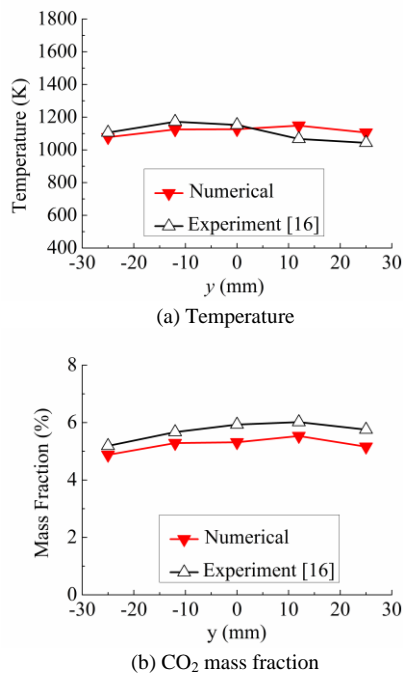


Fig. 2. Temperature and CO₂ mass fraction radial profiles at combustor outlet

V. RESULTS

A. Fuel Droplet Spray and Atomization

When fuel is introduced into the combustor from the nozzle, it is broken up into tiny fuel droplets firstly and then burned with air. The movement of the fuel droplets was traced under 100% load, as shown in Fig. 3. The longest droplet residence time is 2.53ms, which means that fuel is atomized and vaporized quickly and burned immediately after evaporation.

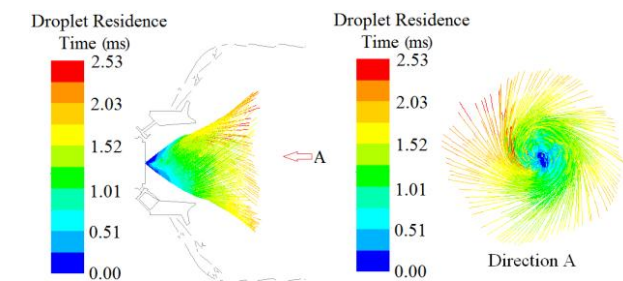


Fig. 3. Fuel droplets path line

B. Velocity Field

Due to little difference on the streamlines of velocity field under the loads from 30% to 100%, only the velocity field in the combustor under full load is presented in this paper, as shown in Fig. 4. It can be seen from the figure that the flow

from the swirler to the combustor outlet can be mainly divided into three zones, namely primary zone, middle zone and mixing zone. In the primary zone, the air leaves the swirler to the combustor liner at high swirling velocity. Then, the air mixes with fuel injected from the nozzle. After that, the swirling mixture of the air and fuel flows forward and entraps the air in the center area of the combustor liner, and at the same time, the downstream air refills the region. As a result, a CRZ (Central Recirculation Zone) with a counter-rotating vortex pair forms in the head of the combustor liner, which ensures ignition and stable combustion in the combustor liner. But due to the non-symmetry of the shell, the flow rates of air flowing into the combustor liner from the upper and lower surfaces are different, so the vortexes are asymmetric. It can also be seen from Fig.4, the gas in CRZ just flows back to the swirler exit which can avoid the phenomenon of flashback occurring. In the downstream area of the primary zone, strong fresh air injects into the combustor liner from the primary holes, as a result, the primary zone is cut off by the fresh air. Although a small amount of the gas is inhaled into the primary zone, most gas flows downstream and mixes with the cold air from the dilution holes. This makes the flow in the combustor more uniform.

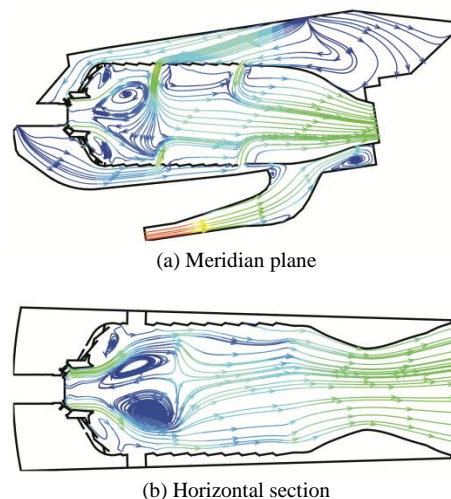


Fig. 4. Streamlines of velocity field in combustor under 100% load

C. The Air Flow Distribution

The air flow distribution is a basic problem in combustor design and development. It affects the combustor ignition, combustion efficiency, flame stability, total pressure loss, wall cooling, outlet temperature distribution and so on. In order to modify the original oil fuel combustor into a dual-fuel one, the air flow distribution in the origin combustor was studied. Fig. 5 shows the proportions of swirler and primary holes air distribution. It can be seen from the figure, the proportion of the air distribution under different conditions is almost the same: swirler air-15%, primary air -29.5%. So it can be concluded that the air distribution is mainly determined by the combustor structure, not the operating conditions.

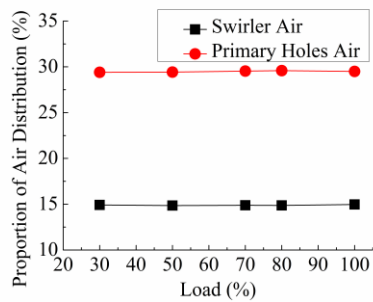


Fig. 5. Air flow distribution under different conditions

D. Pressure Loss

Fig. 6 shows the numerical and experimental data of σ^* (pressure recovery factor) under different conditions, which can reflect the pressure loss directly. As shown in the figure, the numerical data and experimental data show a good agreement and the σ^* slightly increases as the combustor load increases. When the combustor load is 30%, the σ^* of the experiment and simulation are 94.52% and 93.18%, respectively. And when the combustor load is 100%, the σ^* of the experiment and simulation are 94.93% and 94.13%, respectively.

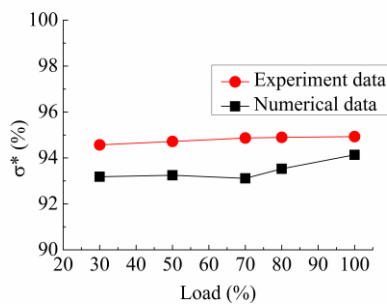


Fig. 6. Pressure recovery factor under different conditions

E. Temperature Field

The contours of the predicted gas temperature for the combustion of $C_{12}H_{23}$ in combustor are shown in Fig. 7. The peak gas temperature is located in the primary zone. However, due to the dilution of burned gas with the air, the gas temperature is lower in middle and mixing zones than that in primary zone. It can be seen from Fig.7, the high temperature zone becomes bigger as the load increases. It is because more fuel is burned in the combustor under the high load. Due to the unsymmetrical flow field in the combustor, the temperature distribution in the combustor is also asymmetric. As can be seen from the Fig.7, the gas temperature near the lower surface of the combustor liner is higher than that near the upper surface in the primary zone. However, the gas temperature near the lower surface of the combustor liner is lower than that near the upper surface in the middle zone and mixing zone. The maximum temperature difference between upper and lower surfaces appears in the middle zone, which is about 400K. In order to protect the combustor liner, a symmetrical flow field is required.

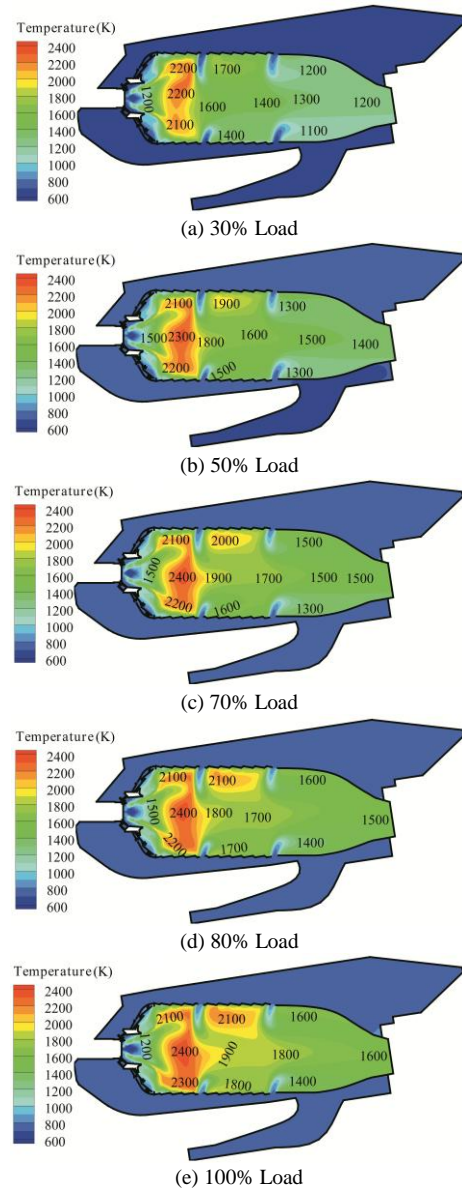
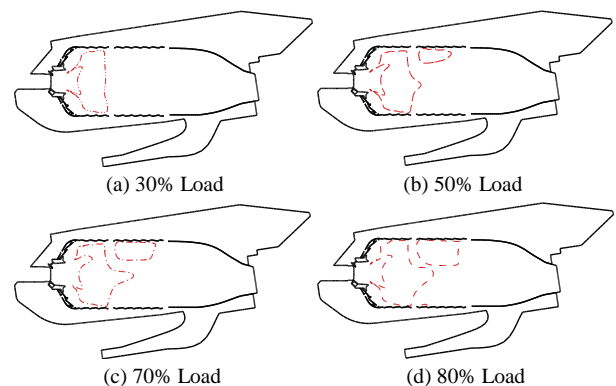


Fig. 7. Temperature field

In order to study the high temperature zone in detail, the contours of $T=1800K$ under different conditions are shown in Fig. 8. As can be seen from Fig. 8, there are two high temperature zones in the combustor. One is the CRZ, which increases as the load increases along the central axis of combustor liner. The other locates behind the primary holes, which is not existence under 30% load but becomes biggest under full load.



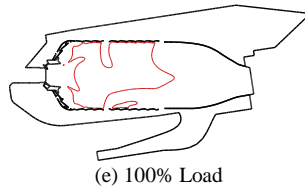


Fig. 8. Contours of $T=1800K$ under different conditions

The temperature distribution along the central axis of combustor liner is shown in Fig. 9. As seen in the figure, due to more fuel burned under the high load, the outlet temperature increases as the load increases. In the region from the fuel nozzle to $x=0.15m$, due to the atomization and evaporation processes of fuel, the temperature at the central axis of combustor liner has little change as the load increases. However, in the region from $x=0.15m$ to combustor outlet, the temperature at the central axis of combustor liner increases as the load increases. It can also be seen from Fig. 9, due to the air from the primary holes takes more heat to reach the equilibrium temperature, the temperature at the central axis decreases sharply at $x=0.2 \sim 0.22m$. At $x=0.35m$, the temperature at the central axis decreases under all conditions which illustrates that the air from dilution holes can blend with the burned gas effectively. And the mixing of dilution air and burned gas is useful to improve the uniformity of combustor outlet temperature distribution.

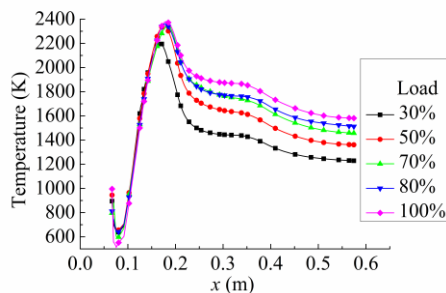


Fig. 9. Temperature distribution along the central axis

F. NO_x Emission

In this paper, in order to modify an oil combustor into a dual-fuel combustor and control the NO_x emission at the same time, the NO_x emission performance of the origin combustor was studied here. The thermal NO_x and prompt NO_x were considered in this paper. Fig. 10 shows the formation rates of thermal and prompt NO along the central axis of combustor liner under 100% load. As can be seen from the figure, the maximum formation rate of prompt NO is far less than that of the thermal NO, which are 5.56×10^{-6} and $0.091 \text{ kmol m}^{-3} \text{ s}^{-1}$, respectively. It illustrates that the thermal NO_x emission is the mainly NO_x emission in this combustor. Fig. 11 shows the formation rates of NO along the central axis of combustor liner under different conditions. The formation rate of NO including the formation rates of thermal NO and prompt NO. It can be seen from the figure, the maximum formation rate of NO under each condition is located in the primary zone and the maximum formation rate of NO increase as the load increases. This is mainly due to the temperature increases as the load increases. It can also be seen from Fig. 11, the maximum formation rate of NO under 30% load is far less than that under 100% load, which are 0.012 and 0.091

$\text{kmol m}^{-3} \text{ s}^{-1}$, respectively.

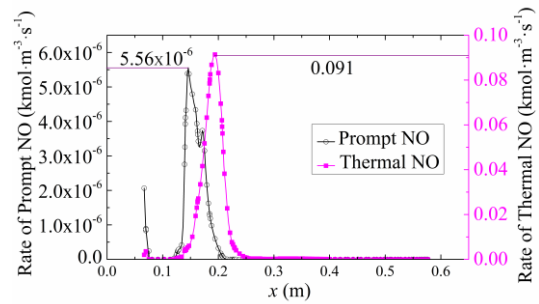


Fig. 10. Rate of thermal and prompt NO along the central axis (100% load)

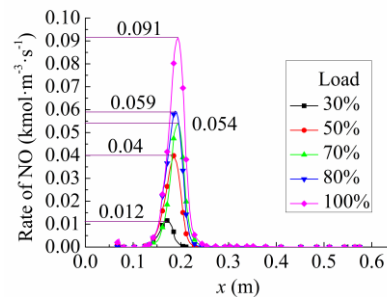


Fig. 11. Rate of NO along the central axis

Fig. 12 shows the NO_x emission at combustor outlet. Due to the formation rate of NO increases as the load increases, the NO_x emission at combustor outlet increases. The lowest NO_x emission is 111.6ppm at 30% load and the highest is 628.9 ppm at 100% load. The NO_x emission of the combustor does not meet the requirements of the regulations. It can be concluded from Figs. 7, 11 and 12 that the higher temperature in the primary zone can lead to higher formation rate of NO, then more NO_x emission at the combustor outlet. So in order to modify the origin combustor into a dual-fuel one with low NO_x emission, some effective measures should be adopted to control the temperature in the primary zone of this combustor.

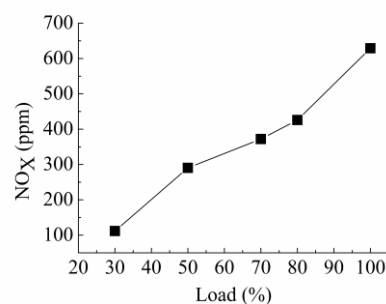


Fig. 12. NO_x emission at combustor outlet under different conditions

VI. CONCLUSION

In order to design a dual-fuel combustor for the CRGT, three-dimensional CFD analysis of $C_{12}H_{23}$ combustion in gas turbine can annular combustor is presented in this study. The effects of different conditions on the flow field, flame shape, gas temperature and NO_x emission were determined in this study. The obtained results were in good agreement with other experimental results. The results derived in this paper are listed briefly as follows:

1) The combustor burns fuel effectively under different conditions. A CRZ with two unsymmetrical vortices is

created in combustor, which could improve the flame stability under different conditions.

2) Due to the unsymmetrical flow field, the temperature distribution in combustor is asymmetrical also. The gas temperatures near the upper and lower surfaces of combustor liner are different, and the maximum temperature difference is about 400K in the middle zone, which is not conducive to protect the liner. So a symmetrical flow field in the combustor may extend the life of the combustor liner.

3) The NO_x emission at the combustor outlet monotonous increases as the load increases. The values of the NO_x emission are 628.9 ppm and 111.6ppm under 100% load and 30% load, respectively. In order to reduce the NO_x emission, an effective way should be adopted to lower the temperature in the primary zone.

In summary, in order to modify the oil combustor into a dual-fuel one successfully, the high NO_x emission problem of the oil combustor must be solved.

dissertation, Nanjing University of Aeronautics and Astronautics, Nanjing, 2009.

REFERENCES

- [1] L. G. Alves and S. A. Nebra, "Thermoeconomic Evaluation of a Basic Optimized Chemically Recuperated Gas Turbine Cycle," *International Journal of Thermo-dynamics*, vol. 6, no. 1, pp.13–22, 2003.
- [2] R. Carapellucci and A. Milazzo, "Thermodynamic optimization of a reheat chemically recuperated gas turbine," *Energy Conversion and Management*, vol. 46, no. 18-19, pp. 2936–2953, 2005.
- [3] C. Luo, N. Zhang, N. Lior and H. Lin, "Proposal and analysis of a dual-purpose system integrating a chemically recuperated gas turbine cycle with thermal seawater desalination," *Energy*, vol. 36, no. 6, pp. 3791–3803, 2011.
- [4] W. Han, H. Jin, N. Zhang and X. Zhang, "Cascade utilization of chemical energy of natural gas in an improved CRGT cycle," *Energy*, vol. 32, no. 4, pp. 306–313, 2007.
- [5] L. Li, X. F. Peng and T. Liu, "Combustion and cooling performance in an aero-engine annular combustor," *Applied Thermal Engineering*, vol. 26, pp.1771–1779, 2006.
- [6] J. C. Chen and W. Chen, "How flow becomes turbulent," *IAENG International Journal of Applied Mathematics*, vol. 42, no. 2, pp.99–110, 2012.
- [7] L. A. Danao, J. Edwards, O. Eboibi and R. Howell, "A Numerical Investigation into the Effects of Fluctuating Wind on the Performance of a Small Scale Vertical Axis Wind Turbine," *Engineering Letters*, vol. 21, no. 3, pp. 149–157, 2013.
- [8] H. Wang, K. Luo, S. Lu and J. Fan, "Direct numerical simulation and analysis of a hydrogen/air swirling premixed flame in a micro combustor," *International Journal of Hydrogen Energy*, vol. 36, no. 21, pp.13838–13849, 2011.
- [9] P. Gobatto, M. Masi, A. Toffolo and A. Lazzaretto, "Numerical simulation of a hydrogen fuelled gas turbine combustor," *International Journal of Hydrogen Energy*, vol. 36, no. 13, pp.7993–8002, 2011.
- [10] C. Ghenai, "Combustion of Syngas Fuel in Gas Turbine Can Combustor," *Advances in Mechanical Engineering*, vol. 2010, pp.1–13, 2010.
- [11] R. C. Orbay, K. J. Nogenmyr, J. Klingmann and X. S. Bai, "Swirling turbulent flows in a combustion chamber with and without heat release," *Fuel*, vol. 104, pp. 133–146, 2013.
- [12] J. Wan, A. Fan, K. Maruta, H. Yao and W. Liu, "Experimental and numerical investigation on combustion characteristics of premixed hydrogen/air flame in a micro-combustor with a bluff body," *International Journal of Hydrogen Energy*, vol. 37, no. 24, pp. 19190–19197, 2012.
- [13] M. Zhang, Z. Fu, Y. Lin and J. Li, "CFD Study of NO_x Emissions in a Model Commercial Aircraft Engine Combustor," *Chinese Journal of Aeronautics*, vol. 25, pp. 854–863, 2012.
- [14] B. Hu, Y. Huang, F. Wang and F. Xie, "CFD predictions of LBO limits for aero-engine combustors using fuel iterative approximation," *Chinese Journal of Aeronautics*, vol. 26, no. 1, pp. 74–84, 2013.
- [15] *ANSYS Fluent 12.0 Theory Guide*, ANSYS, Inc., January 2009.
- [16] X. X. Dang, "Experimental investigation and numerical simulation of a gas turbine annular combustor with dual-stage swirler," Ph.D.